Multipath-assisted Indoor Positioning Enabled by Directional UWB Sector Antennas

Conference Paper · July 2017

CITATIONS
0

READS
54

5 authors, including:

Michael Rath
Graz University of Technology
5 PUBLICATIONS **3** CITATIONS
SEE PROFILE

Josef Kulmer
Graz University of Technology
15 PUBLICATIONS **89** CITATIONS
SEE PROFILE

Mustafa S. Bakr
Graz University of Technology
10 PUBLICATIONS **2** CITATIONS
SEE PROFILE

Klaus Witrisal
Graz University of Technology
149 PUBLICATIONS **1,667** CITATIONS
SEE PROFILE

Multipath-assisted Indoor Positioning Enabled by Directional UWB Sector Antennas

Michael Rath, Josef Kulmer, Mustafa S. Bakr, Bernhard Großwindhager, Klaus Witrisal
Graz University of Technology, Austria
email: {mrath, kulmer, mustafa.bakr, grosswindhager, witrisal}@tugraz.at

***Abstract*—High-accuracy indoor radio positioning can be achieved by using high signal bandwidths to increase the time resolution. Multiple fixed anchor nodes are needed to compute the position or alternatively, reflected multipath components can be exploited with a single anchor. In this work, we propose a method that explores the time and angular domains with a single anchor. This is enabled by switching between multiple directional ultra-wideband (UWB) antennas. The UWB transmission allows to perform multipath resolved indoor positioning, while the directionality increases the robustness to undesired, interfering multipath propagation with the benefit that the required bandwidth is drastically reduced. The positioning accuracy and performance bounds of the switched antenna are compared to an omni-directional antenna. Two positioning algorithms are presented based on different prior knowledge available, one using floorplan information only and the other using additionally the beampatterns of the antennas. We show that the accuracy of the position estimate is significantly improved, especially in tangential direction to the anchor.**

***Index Terms*—localization, position error bound, directional antenna, UWB, multipath component.**

I. Introduction

Accurate radio positioning for indoor environments can be achieved with time-of-flight methods based on (ultra-) wideband signals. In harsh scenarios, the dense multipath propagation can significantly deteriorate the probing signals. To tackle this issue, one can increase the signal bandwidth, allowing for an increased time resolution such that the interfering multipath is resolved in time from the useful line-of-sight (LOS) component [1]. At ultra-wide bandwidth (UWB), one can even exploit multipath, turning a foe into a friend [2]. This makes it possible to reduce infrastructure and to gain robustness in non-line-of-sight situations.

Alternatively, multiple measurements can be combined to resolve the multipath in the angular domain, which reduces the bandwidth required to achieve a desired accuracy. This can be achieved by combining signals originating from different transmitters distributed over the environment, or by using array processing techniques where the measurements of many omni-directional antennas are used. The latter case, using wideband antennas, is well known to yield highly accurate position measurements [3], [4], [5, Chapter 18]. However, both approaches require a lot of infrastructure and coherent processing of the received signals.

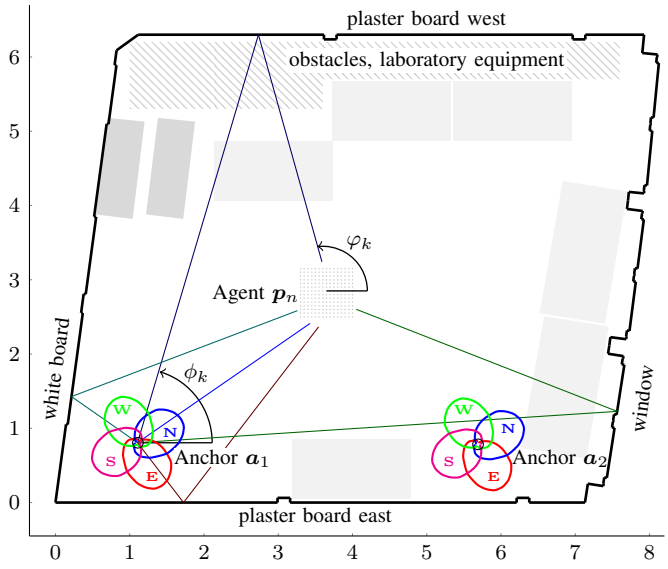

Fig. 1. Floorplan of measurement environment. Tables (light-gray) and cupboards (dark-gray) are shown, as well as patterns of the used antennas at the anchors. The axis describes the distance in meters.

We propose employing multiple switched directional antennas which are capable of UWB transmissions [6]. The antennas are connected to a single transceiver, which will be used as an anchor, for instance. Each employed antenna covers (e.g.) a part of the azimuth plane. Due to the UWB transmission, their measurements can be used to perform multipath-resolved positioning where detectable multipath components (MPC) are associated with the environment. The directional antenna reduces interfering multipath and thus the required bandwidth to be able to resolve MPCs. We analyze the achieved positioning accuracy using directional antennas in comparison with an omni-directional one. We also derive algorithms for this new type of radio frontend. Both results are validated using experimental data from a measurement campaign. Directive antennas were also proposed for indoor positioning in [7], [8], however received signal strength measurements are used from narrowband antenna elements to augment angle-of-arrival estimation.

The paper is organized as follows: Section II discusses the

This work was performed in part within the LEAD-Project Dependable Internet of Things in Adverse Environments, funded by Graz University of Technology.

978-1-5090-3009-5/17/$31.00

basic signal model. Section III provides a description of the statistical error bounds for positioning taking the directive antennas into account. Section IV describes the developed positioning algorithms based on the signal model. In Section V we evaluate the performance bounds, likelihood functions and achieved position accuracy with the algorithms based on measurement data. Section VI summarizes the work and presents concluding remarks.

II. Signal Model

We consider an agent node aiming at finding its position $\boldsymbol{p}$ using radio frequency measurements from one anchor node, located at known position $\boldsymbol{a}$. The agent node is equipped with a single omni-directional antenna. The anchor node employs a sector antenna which consists of M directional antennas as illustrated in Fig. 1. Two anchors are shown, equipped with $M = 4$ antennas, each covering one sector of the azimuth angle plane with a half-power beamwidth of about $90°$. Antenna m transmits the signal $s(t)$ and the sampled signal $\boldsymbol{r}_m \in \mathbb{C}^{N\times 1}$ is observed at the agent. We model this received signal as a sum of deterministic MPCs plus contributions of diffuse multipath (DM) $\boldsymbol{\nu}_m$ and additive, white Gaussian noise (AWGN) $\boldsymbol{w}_m$, according to

$$\boldsymbol{r}_m = \sum_{k=1}^{K} \alpha_k b_m(\phi_k)\boldsymbol{s}(\tau_k) + \boldsymbol{\nu}_m + \boldsymbol{w}_m. \tag{1}$$

The first term on the right-hand-side describes the deterministic MPCs as replicas of the transmitted signal $s(t)$. Each replica is delayed by τ_k which is determined by the length of the path between the agent and the anchor. Reflected paths can be modeled by virtual anchors whose positions are computed from the environment model [2], [9]. We use a vector notation with $\boldsymbol{s}(\tau_k) = [s(0\cdot T_s - \tau_k), s(1\cdot T_s - \tau_k), \ldots, s((N-1)\cdot T_s - \tau_k)]^{\mathrm{T}}$ where T_s is the sampling period and the signal is normalized according to $\|s(t)\|^2 = 1$. For each MPC, the environmental model is also used to determine the angle-of-departure at the anchor denoted by ϕ_k, as well as the angle-of-arrival at the agent denoted by φ_k. This is illustrated in Fig. 1, where both angles are shown for the MPC that comes from the "plaster board west" surface. The amplitude of each MPC is determined on the one hand by α_k which covers propagation effects, e.g. path loss or attenuation at the reflection point, and on the other hand by the complex-valued beampattern described by $b_m(\phi_k)$. For simplicity, we consider only the directional characteristics at the anchor side, assuming a uniform radiation pattern at the agent.

The second term of Equation (1) describes the DM which models interfering MPCs that cannot be associated to an environmental model. It is described as a zero-mean Gaussian random process, shaped by the transmitted signal $s(t)$. The AWGN exhibits a constant double-sided power spectral density of $N_0/2$.

III. Position error bound

We use the *position error bound* (PEB) [10] as derived in [2], [11] to analyze the performance gain of the sector antenna when used for multipath-assisted positioning. It is defined as

$$\mathbb{E}\{\|\boldsymbol{p} - \hat{\boldsymbol{p}}\|^2\} \geq \mathrm{tr}\{\boldsymbol{\mathcal{I}}_{\boldsymbol{p}}^{-1}\} \tag{2}$$

where $\mathrm{tr}\{\cdot\}$ denotes the trace operator and $\boldsymbol{\mathcal{I}}_{\boldsymbol{p}}$ is the Fisher information matrix of $\boldsymbol{p}$ written by

$$\boldsymbol{\mathcal{I}}_{\boldsymbol{p}} = \frac{8\pi^2\beta^2}{c^2}\sum_k\sum_m \mathrm{SINR}_{k,m}\boldsymbol{D}_r(\varphi_k). \tag{3}$$

Here, c is the speed of light, β is the mean-square bandwidth of the transmitted pulse and $\boldsymbol{D}_r(\varphi_k) = \boldsymbol{e}(\varphi_k)\boldsymbol{e}(\varphi_k)^{\mathrm{T}}$ is called the ranging direction matrix that is used to relate the ranging information intensity to the direction of φ_k [10]. The contribution of each individual MPC is quantified by its signal-to-interference-plus-noise ratio (SINR) [11], here defined by

$$\mathrm{SINR}_{k,m} = \frac{|\alpha_k|^2|b_m(\phi_k)|^2}{N_0 + T_{\mathrm{p}}\int\limits_{\phi}|b_m(\phi)|^2 S_\nu(\tau_k,\phi)\,\mathrm{d}\phi}$$

where $S_\nu(\tau,\phi)$ describes the angle-delay power spectrum of the DM and T_{p} is a pulse duration parameter of waveform $s(t)$, see [11].

From (3), the gain of exploiting M measurements is seen to be expressed by $\sum_m \mathrm{SINR}_{k,m}$, because $\boldsymbol{D}_r(\varphi_k)$ is the same for all m. This result is based on the assumption that (i) only ranging information is exploited for solving the positioning problem (i.e. angle information is neglected because the angle resolution is assumed to be very coarse), and (ii) the DM and AWGN are independent for individual measurements m. To evaluate the potential performance gain, we assume a uniform angular power spectrum $S_\nu(\tau_k,\phi) = S_\nu(\tau_k)$. Furthermore, since the efficiency of the antenna is not related to its directivity, we assume that its total power gain is independent of the beam pattern, expressed as $\int_{-\pi}^{\pi}|b_m(\phi)|^2\,\mathrm{d}\phi = 1$. We thus get

$$\sum_m \mathrm{SINR}_{k,m} \approx \frac{|\alpha_k|^2}{N_0 + T_{\mathrm{p}}S_\nu(\tau_k)}\sum_m |b_m(\phi_k)|^2 \tag{4}$$

showing that the SINR gain is approximated as the sum of the antenna power gains at ϕ_k.

IV. Derivation of the positioning algorithm

The previous section investigated the signal model and the expected position error using performance bounds. In the following, we derive an algorithm for multipath-assisted indoor localization using a single anchor only. We will exemplify two methods: Algorithm I treats the measurements as independent and Algorithm II incorporates the antenna gain patterns to get the agent's position.

In Algorithm I we assume that the path amplitudes, including the beampatterns, $\alpha_{k,m} = \alpha_k b_m(\phi_k)$, are estimated independently from each measurement m as nuisance parameters. Stacking the signals $\boldsymbol{s}(\tau_k)$ in the signal matrix $\boldsymbol{S}(\boldsymbol{\tau}) = [\boldsymbol{s}(\tau_1),\ldots,\boldsymbol{s}(\tau_K)]$ with the delays $\boldsymbol{\tau} = [\tau_1,\ldots,\tau_K]^{\mathrm{T}}$ and

corresponding the amplitudes in $\boldsymbol{\alpha}_m = [\alpha_{1,m}, \ldots, \alpha_{K,m}]^{\mathrm{T}}$, the signal model is

$$\boldsymbol{r}_m = \boldsymbol{S}(\boldsymbol{\tau})\boldsymbol{\alpha}_m + \boldsymbol{w}_m$$

where we neglect the contribution by the DM. With this AWGN noise model, the likelihood function of the received signal $\boldsymbol{r}_m$ conditioned on $\boldsymbol{\alpha}_m$ and $\boldsymbol{\tau}$ follows as

$$p(\boldsymbol{r}_m|\boldsymbol{\alpha}_m, \boldsymbol{\tau}) \propto \exp\{ - \|\boldsymbol{r} - \boldsymbol{S}(\boldsymbol{\tau})\boldsymbol{\alpha}_m\|^2\}. \tag{5}$$

In order to estimate the agent's position, we express the delays $\boldsymbol{\tau}$ as a function of the agent's position $\boldsymbol{p}$ using the geometric model of the environment. With hypothesized $\boldsymbol{\tau}$, the amplitudes are estimated using least-squares [12]

$$\hat{\boldsymbol{\alpha}}_m = (\boldsymbol{S}^{\mathrm{H}}(\boldsymbol{\tau})\boldsymbol{S}(\boldsymbol{\tau}))^{-1}\boldsymbol{S}^{\mathrm{H}}(\boldsymbol{\tau})\boldsymbol{r}_m. \tag{6}$$

Stacking the measurements in $\boldsymbol{r} = [\boldsymbol{r}_1^{\mathrm{T}}, \cdots, \boldsymbol{r}_M^{\mathrm{T}}]^{\mathrm{T}}$ then the assumption of independent measurements and amplitudes yields

$$p(\boldsymbol{r}|\boldsymbol{p}) = \prod_m p(\boldsymbol{r}_m|\boldsymbol{p})$$

and the maximum likelihood estimation of the agent position $\hat{\boldsymbol{p}}_{\mathrm{Alg1}}$ follows as

$$\hat{\boldsymbol{p}}_{\mathrm{Alg1}} = \underset{\boldsymbol{p}\in\mathcal{P}}{\operatorname{argmax}} \prod_m p(\boldsymbol{r}_m|\boldsymbol{p}) \tag{7}$$

with the set $\mathcal{P}$ containing hypothesized agent positions within the communication range to the anchor.

Algorithm II explicitly employs the complex-valued beampatterns $\{b_m(\cdot)\}$ to estimate the MPC amplitudes α_k jointly from all measurements $m = 1 \ldots, M$ using

$$\boldsymbol{r} = \boldsymbol{X}(\boldsymbol{\tau}, \{b_m(\phi_k)\})\boldsymbol{\alpha} + \boldsymbol{w}$$

where

$$\boldsymbol{X}(\boldsymbol{\tau}, \{b_m(\phi_k)\}) = \begin{bmatrix} b_1(\phi_1)\boldsymbol{s}(\tau_1) & \ldots & b_1(\phi_K)\boldsymbol{s}(\tau_K) \\ \vdots & & \vdots \\ b_M(\phi_1)\boldsymbol{s}(\tau_1) & \ldots & b_M(\phi_K)\boldsymbol{s}(\tau_K) \end{bmatrix}$$

and $\boldsymbol{\alpha} = [\alpha_1, \ldots, \alpha_K]^{\mathrm{T}}$ and $\boldsymbol{w}$ as AWGN. The likelihood function follows in an equivalent fashion as (5) with the ML solution of $\hat{\boldsymbol{p}}_{\mathrm{Alg2}}$ according to

$$\hat{\boldsymbol{p}}_{\mathrm{Alg2}} = \underset{\boldsymbol{p}\in\mathcal{P}}{\operatorname{argmax}}\ p(\boldsymbol{r}|\boldsymbol{p}) \tag{8}$$

where we expressed the conditionals $\boldsymbol{\tau}$ and $\{b_m(\phi_k)\}$ by the agent's position $\boldsymbol{p}$. The amplitudes $\boldsymbol{\alpha}$ result equivalent to (6). Assuming non-overlapping MPCs the amplitudes are

$$\hat{\alpha}_k = \frac{\sum_{m=1}^{M} b_m^*(\phi_k)\boldsymbol{s}^{\mathrm{H}}(\tau_k)\boldsymbol{r}_m}{\sum_{m=1}^{M} |b_m(\phi_k)|^2} = \frac{\sum_{m=1}^{M} b_m^*(\phi_k)\hat{\alpha}_{k,m}}{\sum_{m=1}^{M} |b_m(\phi_k)|^2} \tag{9}$$

with $\hat{\alpha}_{k,m} = \boldsymbol{s}^{\mathrm{H}}(\tau_k)\boldsymbol{r}_m$ at the right-hand-side of (9). It shows that the estimated amplitudes $\{\hat{\alpha}_k\}$ of Algorithm II are a weighted average of the individual amplitudes $\{\hat{\alpha}_{k,m}\}$ in Algorithm I.

V. Evaluation

In this section, we evaluate the derived position performance bound in Section III and the achieved accuracy of the multipath-assisted indoor localization algorithms.

A. Measurement setup

We placed one agent at $\boldsymbol{p}_n$ and two anchors at $\boldsymbol{a}_1$ and $\boldsymbol{a}_2$ as illustrated in Fig. 1. The anchors were equipped with $M = 4$ directive antennas, equally spaced on a circle with radius of 2 cm at center $\boldsymbol{a}$. The antennas were aligned such that their mainlobes point at different directions, named *North* (N), *West* (W), *South* (S) and *East* (E), each 90° apart as illustrated in Fig. 1. The measurements between the agent and each directive antenna were performed using an Ilmsens Correlative Channel Sounder [13]. Subsequently, each measurement was convolved by a raised cosine pulse using a carrier frequency of $f_{\mathrm{c}} = 5.4$ GHz. For a comparison of the impact of bandwidth on the estimated SINRs, we used (i) a pulse duration of $T_{\mathrm{p}} = 0.5$ ns (equivalent to a bandwidth of 2 GHz) with a roll-off factor of $R = 0.5$ and (ii) a pulse duration of $T_{\mathrm{p}} = 2.4$ ns (bandwidth of 500 MHz) with a roll-off factor of $R = 0.9$ which has been found to model Channels 2 and 5 of the recently available DecaWave DW1000 UWB transceiver [14]. We placed the agent at $n \in \{1, \ldots, 210\}$ different positions on a 15×14 grid with 5 cm spacing, resulting in 420 channel measurements. For a comparison, we repeated the experiment using omni-directional antennas on both anchor and agent nodes.

The complex-valued beampattern $b_m(\cdot)$ was available as a codebook in a resolution of 10°. We used linear interpolation to evaluate the beampattern, given a specific angle. The spatial offset between the directive antennas results in a phase shift of the carrier frequency as a function of the MPC angle-of-departure. For simplicity, we considered this phase shift already in the beampattern.

B. Evaluation of performance bounds

We evaluate the SINR values of individual MPCs which quantify their contributions to the PEB in (2) via (3). Tables I and II report the estimated SINR values for selected MPCs for the two anchor positions and the pulse durations of $T_{\mathrm{p}} = 0.5$ ns and $T_{\mathrm{p}} = 2$ ns. The SINRs are reported for each directive antenna based on the estimated amplitudes $\hat{\alpha}_{k,m}$. The SINR of *Sec* is based on amplitude estimation considering the overall amplitude in (9) while *Added* denotes the (not weighted) sum of SINRs of *N+W+S+E* as modeled by (4). For comparison we also show the SINRs for an omni-directional antenna at the anchor (*Omni*).

Comparison of Tables I and II demonstrates that, in general, the SINR increases with higher signal bandwidth, justified by the improved separation of MPCs along the delay domain. Further, we can observe that the SINR of an individual directive antenna (*N*, *W*, *S* or *E*) is strongly dependent on the angle-of-departure of the MPC (see Fig. 1 which exemplifies the beampatterns of the directional antennas in addition to the angle-of-departure of the MPCs).

Table I: SINR in dB of deterministic MPCs for $T_\mathrm{p} = 0.5$ ns, $R = 0.5$ at anchor position $\boldsymbol{a}_1$ (top) and $\boldsymbol{a}_2$ (bottom) of sector antenna north (N), west (W), south (S), east (E). The omni-directional antenna (Omni) is shown for comparison.

anchor position $\boldsymbol{a}_1$

MPC	*N*	*W*	*S*	*E*	*Sec*	*Added*	*Omni*
LOS	30.6	16.4	17.9	11.7	33.0	31.0	25.4
plasterb east	6.3	$-\infty$	$-\infty$	12.1	12.8	13.1	11.0
plasterb west	-1.1	3.4	-5.4	$-\infty$	3.2	5.1	0.3
white board	-1.1	18.3	15.9	-0.4	19.4	20.3	11.1
window	1.2	$-\infty$	-3.3	-1.1	1.1	4.1	0.9
$\mathrm{PEB_r}$ / cm	0.2	0.6	0.6	1.1	0.1	0.2	0.3
$\mathrm{PEB_t}$ / cm	4.4	2.3	3.2	4.6	1.8	1.6	3.2

anchor position $\boldsymbol{a}_2$

MPC	*N*	*W*	*S*	*E*	*Sec*	*Added*	*Omni*
LOS	9.0	21.5	23.6	18.3	27.7	26.5	24.8
plasterb east	-9.3	0.3	1.9	1.8	$-\infty$	6.3	2.6
plasterb west	-5.1	-0.8	$-\infty$	$-\infty$	$-\infty$	0.6	$-\infty$
window	15.2	7.8	-0.1	4.3	15.8	16.3	10.0
$\mathrm{PEB_r}$ / cm	1.0	0.5	0.4	0.7	0.3	0.3	0.4
$\mathrm{PEB_t}$ / cm	3.0	5.3	13.0	9.4	2.8	2.4	5.3

Table II: SINR in dB of deterministic MPCs for $T_\mathrm{p} = 2.4$ ns, $R = 0.9$ at anchor position $\boldsymbol{a}_1$ (top) and $\boldsymbol{a}_2$ (bottom) of sector antenna north (N), west (W), south (S), east (E). The omni-directional antenna (Omni) is shown for comparison.

anchor position $\boldsymbol{a}_1$

MPC	*N*	*W*	*S*	*E*	*Sec*	*Added*	*Omni*
LOS	16.1	11.4	11.5	7.4	14.9	18.7	17.2
plasterb east	3.3	5.6	8.8	9.4	8.4	13.5	3.1
plasterb west	3.2	2.0	$-\infty$	-6.5	3.0	5.9	-0.6
white board	0.5	9.5	8.9	3.5	9.4	13.0	3.4
window	$-\infty$	$-\infty$	-1.1	3.0	$-\infty$	4.5	$-\infty$
$\mathrm{PEB_r}$ / cm	4.4	5.8	5.5	7.3	4.3	2.7	3.9
$\mathrm{PEB_t}$ / cm	20.5	18.9	21.5	18.2	16.9	9.8	28.1

anchor position $\boldsymbol{a}_2$

MPC	*N*	*W*	*S*	*E*	*Sec*	*Added*	*Omni*
LOS	3.8	19.3	18.2	16.2	23.5	22.9	19.4
plasterb east	-2.8	-0.1	1.9	3.4	3.5	7.2	1.4
plasterb west	$-\infty$	-0.4	$-\infty$	-4.4	-0.8	1.0	$-\infty$
window	10.8	2.2	-5.3	3.1	11.6	12.1	4.4
$\mathrm{PEB_r}$ / cm	8.0	3.1	3.6	4.3	1.9	2.0	3.0
$\mathrm{PEB_t}$ / cm	23.2	30.3	76.0	28.0	18.2	15.1	43.6

Consideration of a joint amplitude estimation is highly beneficial in terms of SINR as shown in the *Sec* column. The SINR is clearly improved since it takes information obtained at M measurements into account. The sum of individual SINRs (*Added*) is seen to be an upper limit on the achievable performance. Hereby independent measurements of the DM of each antenna are required.

The tremendous advantage of the directional antennas is the potential to resolve MPCs in the spatial domain. This is justified by Tables I and II by comparison of the SINR values. Consider e.g. the MPCs *plasterb east* and *white board* using anchor position $\boldsymbol{a}_1$. At a high bandwidth of $T_\mathrm{p} = 0.5\,\mathrm{ns}$ (Table I), both MPCs are well separated in the delay domain and subsequently reasonably high SINR values ($> 10\,\mathrm{dB}$) are obtained. The omni-directional antenna reaches similar values compared to the combined sector antennas *Sec*. As soon as the bandwidth is reduced (Table II), both MPCs overlap and

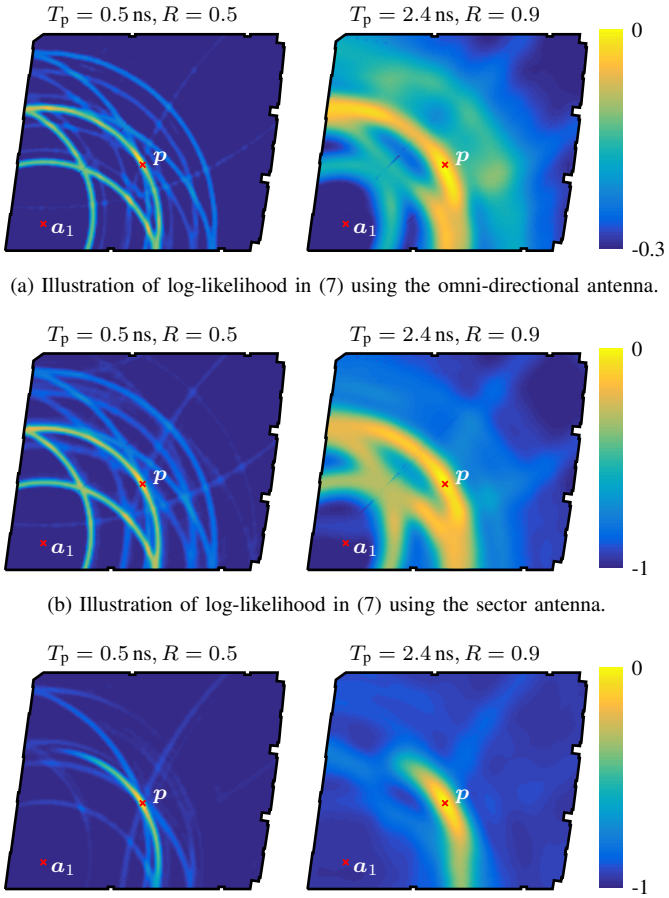

(a) Illustration of log-likelihood in (7) using the omni-directional antenna.

(b) Illustration of log-likelihood in (7) using the sector antenna.

(c) Illustration of log-likelihood in (8) using the sector antenna.

Fig. 2. Illustration of likelihood in log-domain using the sector antenna as function of agent position evaluated for points within the communication range (see Fig. 1). The anchor and *true* agent position are indicated by $\boldsymbol{a_1}$ and $\boldsymbol{p}$.

the SINRs using the omni-directional antenna suffer. Still, the sector antenna is able to gain additional spatial information, verified by the formidable improvement of *Sec* and *Added*.

Finally, we report the evaluated PEB, radial ($\mathrm{PEB_r}$) and tangential ($\mathrm{PEB_t}$) to the angle-of-arrival of the LOS. In general, the PEB is lower in direction of the LOS because the LOS is usually equipped with the highest SINR. Using the sector antennas, the tangential PEB is reduced by up to a factor of three, still employing only one anchor node.

We conclude that the SINR is strongly dependent on the beampattern as well as the bandwidth. MPCs having an angle-of-departure within the antenna's mainlobe reach high SINRs. The combination of the antennas is superior since more channel measurements are used in combination with angular diversity.

C. Evaluation of the likelihood functions

Fig. 2 illustrates the likelihood functions in log-domain using $\boldsymbol{a}_1$ and pulse parameters of $s(t)$ with high bandwidth $(T_\mathrm{p}, R) = (0.5\,\mathrm{ns}, 0.9)$ and low bandwidth $(2.4\,\mathrm{ns}, 0.5)$ for positions within the communication range (compare to floorplan in Fig. 1). Brighter areas indicate a better model fit. We

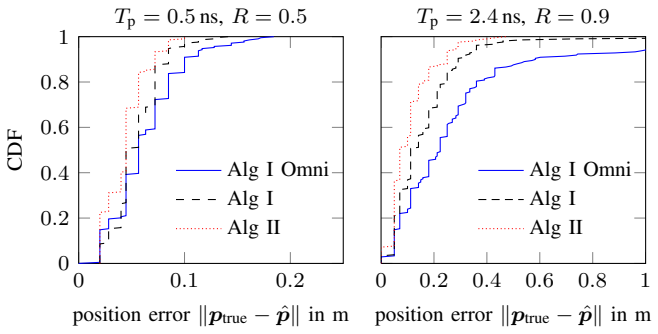

Fig. 3. Cumulative distribution function (CDF) of the position error using pulse parameters $(T_\mathrm{p}, R) = (0.5\,\mathrm{ns}, 0.9)$ (left) and $(2.4\,\mathrm{ns}, 0.5)$ (right) of Algorithm I and II. Algorithm I Omni incorporates a single omni-directional antenna and is shown for comparison.

can observe that increased bandwidth (left) yields a steeper likelihood. The angular diversity of the sector antenna using Eq. (7) (Fig. 2b) and (8) (Fig. 2c) reduces some of the local maxima and thus the probability for outliers (Fig. 2a). The estimation of $\{\alpha_k\}$ in (8) (Fig. 2c) results in a more distinct likelihood function compared to the independent estimation of $\{\alpha_{k,m}\}$ in (7) (Fig. 2a). Especially for $T_\mathrm{p} = 2.4\,\mathrm{ns}$ the application of the directional antennas results in a distinct global maximum that is well separated from the local maxima as shown in Fig. 2c.

D. Evaluation of the position accuracy

Finally, we investigate the performance of both position estimators using anchor $\boldsymbol{a}_1$ and 210 measurements of $\{\boldsymbol{r}_m\}$ each at a different position of $\boldsymbol{p}$. All measurements were performed in LOS conditions, considering the MPCs evaluated in Tables I and II. The cumulative distribution functions of the distance between the *true* and estimated positions $\epsilon = \|\boldsymbol{p}_\mathrm{true} - \hat{\boldsymbol{p}}\|$ are shown in Fig. 3. It confirms that a high bandwidth (Fig. 3 left) is favorable for indoor positioning, with 90% of ϵ below 10 cm. This reveals that the high bandwidth suffices to separate and utilize the multipath propagation.

Using a lower bandwidth (Fig. 3 right) exemplifies the gain due to the directional antennas compared to the omni-directional antenna. The omni-directional antenna is not able to separate the MPCs well enough (compare the likelihood function in Fig. 2a right) which results in a poor position error where the 90% limit of ϵ is only at 50 cm. Using the sector antenna drastically reduces the position error. Algorithm 1 gathers additional information due to angular diversity. The incorporation of the beampattern by Algorithm II enables highly accurate indoor localization where the 90% limit of the position error is reduced to 20 cm.

VI. Conclusions

In this paper, we have evaluated a UWB indoor positioning system using multiple directive UWB sector antennas at the anchor side. We included the antenna patterns into theoretical performance bounds for positioning and, based on that, we analyzed the reliability of deterministic MPCs in comparison with the performance of an omni-directional antenna. Two positioning algorithms were presented, both described by ML estimators using the measurements of the directive antennas and the floorplan information. The second algorithm also made use of the directive antenna patterns. The accuracy of both algorithms was evaluated by examining the likelihood functions and the cumulative distribution function of the position error. It was shown that the directive antennas achieve overall better results, especially considering the tangential information of the MPC directions.

References

[1] K. Witrisal, E. Leitinger, S. Hinteregger, and P. Meissner, "Bandwidth scaling and diversity gain for ranging and positioning in dense multipath channels," *IEEE Wireless Communications Letters*, vol. 5, no. 4, pp. 396–399, Aug 2016.

[2] K. Witrisal, P. Meissner, E. Leitinger, Y. Shen, C. Gustafson, F. Tufvesson, K. Haneda, D. Dardari, A. F. Molisch, A. Conti, and M. Z. Win, "High-accuracy localization for assisted living," *IEEE Signal Processing Magazine*, 2016.

[3] Y. Shen and M. Z. Win, "On the accuracy of localization systems using wideband antenna arrays," *IEEE Transactions on Communications*, vol. 58, no. 1, pp. 270–280, January 2010.

[4] Y. Han, Y. Shen, X. P. Zhang, M. Z. Win, and H. Meng, "Performance limits and geometric properties of array localization," *IEEE Transactions on Information Theory*, vol. 62, no. 2, pp. 1054–1075, Feb 2016.

[5] B. Allen, M. Dohler, E. Okon, W. Malik, A. Brown, and D. Edwards, *Ultra wideband antennas and propagation for communications, radar and imaging*. John Wiley & Sons, 2006.

[6] B. Großwindhager, M. S. Bakr, M. Rath, F. Gentili, W. Bösch, K. Witrisal, C. A. Boano, and K. Römer, "Switchable Directional Antenna System for UWB-based Internet of Things Applications," in *International Conference on Embedded Wireless Systems and Networks (EWSN)*, 2017.

[7] A. Cidronali, S. Maddio, G. Giorgetti, and G. Manes, "Analysis and performance of a smart antenna for 2.45-ghz single-anchor indoor positioning," *IEEE Transactions on Microwave Theory and Techniques*, vol. 58, no. 1, pp. 21–31, 2010.

[8] G. Giorgetti, S. Maddio, A. Cidronali, S. Gupta, and G. Manes, "Switched beam antenna design principles for angle of arrival estimation," in *Wireless Technology Conference, 2009. EuWIT 2009. European*. IEEE, 2009, pp. 5–8.

[9] J. Kunisch and J. Pamp, "An ultra-wideband space-variant multipath indoor radio channel model," in *IEEE Conference on Ultra Wideband Systems and Technologies*, 2003.

[10] Y. Shen and M. Win, "Fundamental limits of wideband localization; part I: a general framework," *IEEE Transactions on Information Theory*, 2010.

[11] E. Leitinger, P. Meissner, C. Ruedisser, G. Dumphart, and K. Witrisal, "Evaluation of position-related information in multipath components for indoor positioning," *IEEE Journal on Selected Areas in Communications*, 2015.

[12] G. H. Golub and V. Pereyra, "The differentiation of pseudo-inverses and nonlinear least squares problems whose variables separate," *SIAM Journal on numerical analysis*, vol. 10, no. 2, pp. 413–432, 1973.

[13] R. Zetik, J. Sachs, and R. S. Thoma, "Uwb short-range radar sensing - the architecture of a baseband, pseudo-noise uwb radar sensor," *IEEE Instrumentation Measurement Magazine*, vol. 10, no. 2, pp. 39–45, April 2007.

[14] J. Kulmer, S. Hinteregger, B. Großwindhager, M. Rath, M. Bakr, E. Leitinger, and K. Witrisal, "Using DecaWave UWB Transceivers for High-accuracy Multipath-assisted Indoor Positioning," in *IEEE ICC 2017 Workshop on Advances in Network Localization and Navigation (ANLN)*, 2017.